ESD Behavior of MWCNT Interconnects—Part II: Unique Current Conduction Mechanism

Abhishek Mishra, *Student Member, IEEE*, and Mayank Shrivastava, *Senior Member, IEEE*

(Invited Paper)

***Abstract*—High-current carrying capacity and superior thermal conductivity have made multiwall carbon nanotubes (MWCNTs) a material for next-generation interconnects. Its distinct electrical and thermal properties result in various physical phenomenon, interaction among which give rise to unique electro-thermal transport. The interaction aggravates in presence of high-electric fields, which generally occur under ESD conditions. In this paper, we present detailed investigation of electro-thermal transport through MWCNTs under ESD conditions. The role of the substrate, MWCNT shells, and sub-bands in ESD current conduction is highlighted, while considering two device architectures—suspended and dielectric-supported MWCNTs. The quantum electron–phonon transport under non-equilibrium (ESD) conditions is explained using CNT band structure and interplay between electrical and thermal transport along the nanotube. The investigation highlights the role of the dielectric substrate in mitigating the detrimental effects of ESD stress. A strong dependence of failure current on metal-MWCNT contact resistance is revealed. The overall breakdown mechanism is found to follow Wunsch–Bell model, indicating a direct scaling between the rate of oxidation of MWCNT shells and injected power.**

***Index Terms*—MWCNT, interconnects, ESD, reliability, electro-thermal transport.**

I. Introduction

EXTRAORDINARY high electrical mobility and thermal conductivity of multiwall carbon nanotubes (MWCNTs) have made them a possible replacements of future interconnects [1], [2]. Their benefits include high current carrying capacity, resistance to electro-migration, high thermal conductivity and high strength due to strong sp^2 bonds between carbon atoms [3]. Conduction of current densities as high as $10^9 A$ across a cross-sectional area of 1 cm^2 have been reported [4], which is two orders of magnitude higher than that of conventional metal interconnects. This emerging material has attracted promising inputs and developments from almost all corners of the fraternity. Compact models [5], various reliability theories [6] and fabrication processes [7] are already available. In spite of various lucrative features, the potential reliability issues like ESD cannot be avoided. A typical ESD event causes co-existence of high current densities and high electric fields at elevated temperatures, which can initiate catastrophic events like oxidation of carbon shells [8], [9] or electro-migration [10] of metal contacts. These events arise due to field-assisted increase in electron-lattice scattering and consequent rise in phonon population. According to scattering model of electrons and phonons, the presence of high electric fields under ESD conditions populate the MWCNT channel with high-energy and slow decaying optical phonons. The consequent rise in local population of out-of-equilibrium phonons, leading to formation of hot-spot, equilibrate by emitting acoustic phonons. The resultant rise in thermal energy spreads in the entire system in a time duration decided by thermal diffusion time of the MWCNT. For a typical micron long MWCNT, this time duration corresponds to few tens of nanoseconds [11]. Since a typical ESD event also lasts for a similar duration, therefore thermal transport is expected to cause transient changes in conduction of ESD current, which can be revealed by time-resolved investigations. Such investigations are vital to the understanding of electro-thermal transport during an ESD event. In this work, we report the ESD-induced electro-thermal effects in MWCNT interconnects and their dependence on various device parameters.

Manuscript received May 17, 2017; revised July 3, 2017; accepted August 2, 2017. Date of publication August 11, 2017; date of current version December 7, 2017. This work was supported by the Department of Science and Technology, Govt. of India, under Grant SB/S3/EECE/063/2014. *(Corresponding author: Abhishek Mishra.)*

A. Mishra is with the Department of Electronic Systems Engineering, Indian Institute of Science, Bengaluru 560012, India, and also with the Center for Nanoscience and Engineering, Indian Institute of Science, Bengaluru 560012, India (e-mail: mishra@iisc.ac.in).

M. Shrivastava is with the Department of Electronic Systems Engineering, Indian Institute of Science, Bengaluru 560012, India (e-mail: mayank@iisc.ac.in).

Color versions of one or more of the figures in this paper are available online at http://ieeexplore.ieee.org.

Digital Object Identifier 10.1109/TDMR.2017.2738701

II. Device Fabrication and Measurement Setup

MWCNTs used in this work were grown by thermal CVD of ferrocene and toluene at a temperature of 850^oC [8]. Post growth tubes were deposited through the process of dielectrophoresis, which involves use of AC signal to align MWCNTs suspended in organic solvent, across metal electrodes [7], [12]. An AC signal of 10 Vpp and 10 MHz was applied across the pair of metal electrodes with various channel lengths. Electrodes used here consists of a stack of chrome-palladium on SiO_2, pre-patterned using electron-beam lithography. Post-dielectrophoresis, the devices were properly cleaned with acetone/IPA, followed by dehydration bake at 250^oC to remove any organic contamination. This deposition technique was selected as it results in side-contacted tubes. Such a contact is best suited for investigating current conduction mechanism through individual shells as only the outermost shell is electrically and physically connected to the

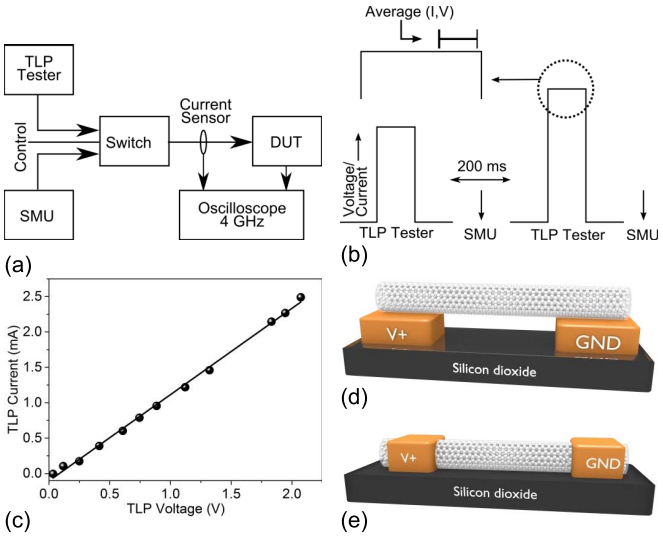

Fig. 1. (a) Experimental setup for emulating ESD stress through MWCNTs. All cables and ports are 50 Ω matched, and the system operates at a bandwidth of 4 GHz. (b) Analysis technique: low-bias (500 mV) DC current is measured after each pulse, while the response towards pulse-voltage is averaged in a window from 70% to 90% of the pulse width. (c) TLP characteristic of an SMD resistor. The curve shows linear behavior in both sub-mA and mA range. Schematic of suspended MWCNT (d) and dielectric-supported MWCNT (e) used in this work.

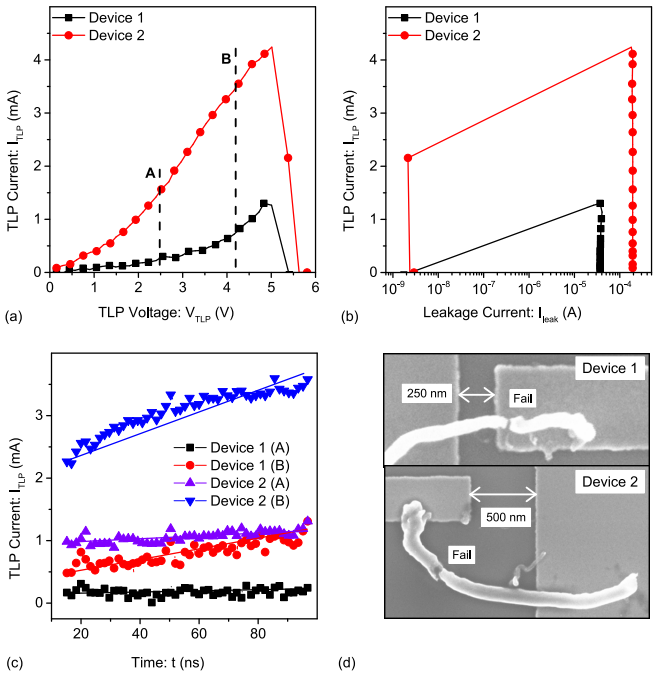

Fig. 2. (a) TLP I-V characteristics of suspended tubes (b) change in low-bias leakage with TLP current (c) Transient waveforms at two different TLP voltages marked in (a). Note that current remains relatively constant with time at bias point marked A, while at point B, it increases linearly with time. (d) SEM image of Device 1 and Device 2 after shell-by-shell failure. Both the devices are suspended between metal electrodes. Note that the devices have failed near contact, indicating ballistic transport through the tube.

metal contact, while the inner-shells participate in conduction via inter-shell tunneling. Two different configurations of side-contacted tubes were selected for TLP measurements (1) short suspended tubes (2) long dielectric-supported tubes. The former configuration does not contact the substrate, while a major fraction of the length of latter configuration rests on the dielectric substrate. ESD investigations were performed using a TLP setup with ultra-low current (~50 μA) sensing capability (figure 1). Low current was sensed by using - 1) inductive current sensor with sensitivity of 5 mV/mA; 2) mixed-domain oscilloscope with resolution of 1 mV/div. Before measurements, the TLP system was well calibrated against a standard SMD resistor and Zener diode. The current sensor shows low-frequency roll-off for pulse-widths of more than 6.3 μs (L/R time constant). Measurements reported in the work were done for pulse-widths $\leq$ 1000 ns, therefore the low-frequency effects (droop) are safely neglected.

Unless stated otherwise, pulse width of 100 ns and rise time of 1 ns are used for all the measurements. To study failure, low-bias device resistance was closely monitored after every ESD stress pulse (figure 1). Since the interconnects based on MWCNTs are still in budding stage and need more improvements at process and modeling fronts, therefore, instead of reporting current per unit footprint, raw TLP current is reported. Nevertheless, the TLP current can be converted to current per unit footprint by using footprint area of $L \times d$, where L and d denotes length and diameter of the tube respectively.

III. Conduction Through Suspended MWCNTs

Figure 2 shows TLP I-V characteristics of suspended MWCNTs and highlights the following key features (1) rise in TLP current shifts from linear to exponential after a particular threshold voltage, (2) current w.r.t. time remains unchanged during the linear branch of the TLP current-voltage characteristics, while it increases linearly with time for currents in the exponential branch of the TLP current-voltage characteristics. The transient increase in current indicates a role of time-dependent phenomenon in the conduction of ESD current. In order to investigate the transient behavior under ESD conditions, Landauer's formulation [13] for electrical conduction through individual shells of MWCNT is referred.

$$I = \frac{2e}{h} TM(\mu_1 - \mu_2) \tag{1}$$

where, $(\mu_1 - \mu_2)$ = TLP voltage, T is the transmission coefficient through the nanotube and M is the number of conduction channels, and h is the Planck's constant. Unlike bulk materials, the circumferential quantization in these materials results in a series of sub-bands. The sum of these sub-bands, weighted with Fermi-Dirac function, defines the number of conduction channels available for conduction. Analytically, for a shell with diameter D, the number of channels participating in conduction at temperature T is given by [5]

$$M(D, T) = aT + b \tag{2}$$

where, a and b are constants, whose values depend on thermal energy of electrons and gap between sub-bands. Consequently, number of conduction channels and hence electrical current (eq. (1)) through the tube depends linearly on temperature and hence, any transient change in temperature can result in transient change in current. Temperature rise due to increase in

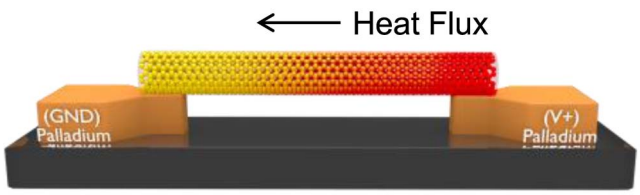

Fig. 3. Heat transport from hot contact ($V+$) to cold contact (GND). The propagation starts at $t = 0^+$ and continues till a state of thermal equilibrium is reached. Hot and cold refers to energy of carriers at the respective electrodes.

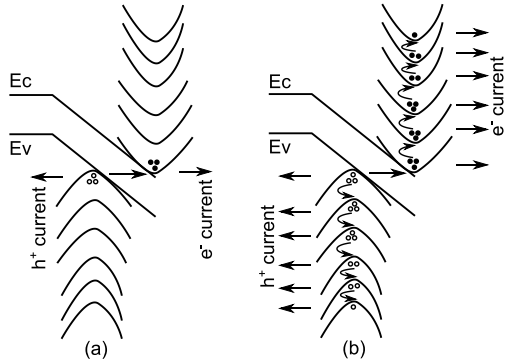

Fig. 4. Occupancy of sub-bands at (a) $t = 0^+$ and (b) $t \geq t_{equilibrium}$. Band diagrams are shown for interface at the cold contact.

thermal energy in MWCNTs is mainly attributed to excitation of optical phonons by energetic electrons. The generated heat creates a region of thermal non-equilibrium, which in turn equilibrate by diffusing heat to regions with low-energy phonons, over a time duration decided by thermal diffusion time of the device. Under high ESD stress conditions, the hot-contact of suspended tube sustains heavy scattering of energetic carriers with the lattice, due to which the contact becomes a reservoir of out-of-equilibrium phonons. Since, relatively less scattering happens at the cold electrode, therefore it acts as a sink for phonons. The difference in phonon population drives heat flux from hot to cold contact, along length of the tube (figure 3). Note that in spite of metal electrode at the hot-contact, which acts as an efficient heat sink, a fraction of heat propagates from hot to cold contact. This flow of heat or thermal energy happens because of the existence of thermal interface resistance at MWCNT-metal interface [14] and high thermal conductivity of MWCNTs. The consequent heating-up of cold contact results in linear increase in number of conduction channels and current, as predicted by equations (1) and (2). This process continues during the entire state of thermal non-equilibrium. The other key feature of the TLP I-V characteristics shown in figure 2 is the exponential rise in current with voltage. Conduction through individual shells of a CNT happens via band-to-band tunneling of electrons from valence band to conduction band (figure 4). The two requirements of tunneling are (1) band-bending enough to cause sufficiently high probability of tunneling, (2) empty states in conduction band and filled states in valence band. The former condition requires a threshold voltage above which current rises exponentially, while requirement of the latter condition is fulfilled by thermal-assisted rise in number of conduction channels as explained earlier. The overall conduction mechanism follows thermal assisted band-to-band tunneling, a mechanism unique to multiwall carbon nanotubes (figure 4). At time $t = 0^+$, depending on temperature and diameter, $S1$ number of sub-bands participate in conduction. Conduction at this instant happens primarily due to direct transmission through crossing sub-bands and tunneling through nearest available non-crossing sub-bands [15]. As explained earlier, temperature of the cold contact keeps increasing due to flux of heat from hot to cold contact. Increase in temperature smears-up the Fermi-Dirac distribution of electrons, and increases the number of sub-bands to $S2$ ($> S1$). Consequently, more states become available for tunneling, which eventually results in exponential rise in current. This process continues till $t = t_{equilibrium}$, at which the device attains thermal equilibrium and stops any further increase in participation of sub-bands.

IV. Conduction Through Dielectric-Supported MWCNTs

The substrate plays a crucial role in deciding thermal and electrical transport through MWCNTs. Underlying substrate not only increases scattering, but also provides a medium for heat dissipation from MWCNT to the substrate. Hence, it is imperative to study the effect of substrate on conduction of ESD current. Figure 5 shows TLP I-V characteristics of dielectric-supported MWCNTs. Similar to suspended tubes, the dielectric-supported tubes also show exponential dependence with voltage and linear rise with time, but the effect is much less pronounced and shows delayed onset. Suspended tubes show increment in current around the TLP voltage of 4 V (figure 2), while current through the dielectric-supported tubes increase around 10 V (figure 5). The reduction in effect is attributed to underlying substrate, which plays a vital role in cooling down the tube. Coupling between hot carriers in the nanotube and polar SiO_2 substrate takes away a major fraction of heat to substrate [16]. Hot, energetic electrons in dielectric-supported nanotube dissipate their energy directly to phonon modes of the underlying polar substrate. Rate of transfer of energy through this process is more than that of energy transfer to optical phonons of the nanotube lattice, consequently former process dominates over the latter and temperature of the nanotube does not rises in spite of conducting large amount of current through diffusive transport [17].

Since hot electrons get de-energize due to underlying polar substrate, compared to suspended tube, the temperature of hot contact in dielectric-supported tube shows relatively less increment and happens at higher TLP voltages. Consequently, the dielectric-supported tube shows relatively less rise in current. Moreover, since the cold contact does not heats-up significantly, therefore, Fermi-Dirac distribution does not smears-in higher sub-bands, which in-turn results in conduction through lower sub-bands only. Figure 6 compares the TLP I-V characteristics of suspended MWCNTs with dielectric-supported MWCNTs and highlights the higher breakdown voltage, but relatively less current in case of dielectric-supported CNTs. The reason behind this observation is attributed to interaction

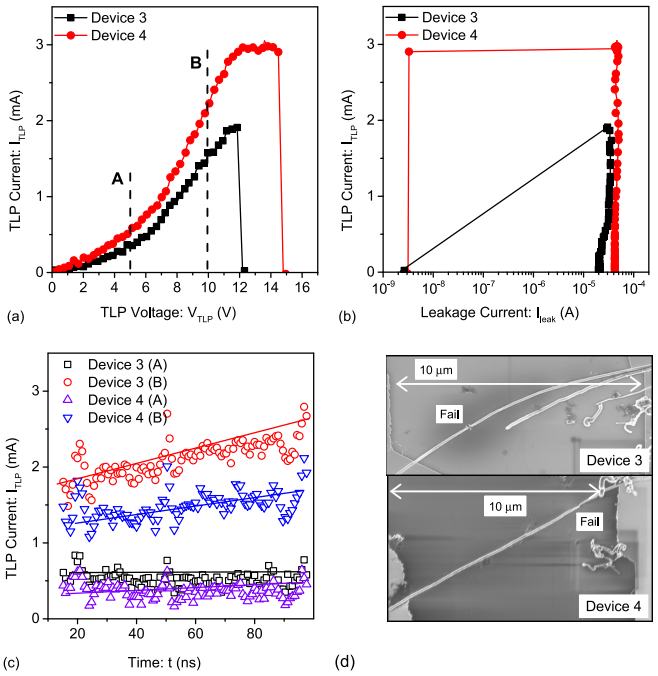

Fig. 5. (a) TLP I-V characteristics of dielectric-supported tubes (b) change in low-bias DC current w.r.t. TLP current (c) Transient waveforms at two different TLP voltages marked in (a). Unlike suspended tubes, the transient rise in collapsed tubes is relatively less pronounced and happens at much higher voltage. (d) SEM image of Device 3 and Device 4. Both the devices are resting on SiO_2.

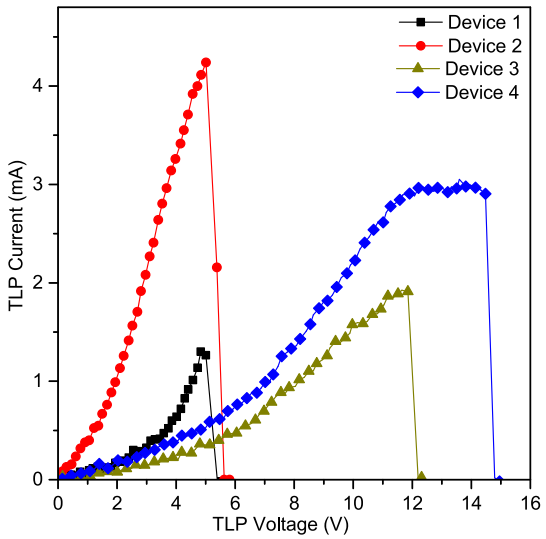

Fig. 6. Comparison of TLP I-V characteristics of suspended tubes (Device 1 and Device 2) with dielectric-supported tubes (Device 3 and Device 4). Compared to suspended tubes, the dielectric-supported tubes show higher breakdown voltage and carry relatively less amount of current.

of energetic electrons with substrate, which results in - 1) transfer of heat to the substrate and increase in the breakdown voltage, as lattice heats-up at higher voltages 2) lower current compared to suspended tubes, because of de-energization of electrons along the length of the tube and conduction through lower-sub-bands only. Moreover, the dielectric-supported tubes show a distinct saturation in current in pre-breakdown region, while the suspended tubes does not show any such saturation. The saturation in current is attributed to scattering due to surface phonons, which is dominant in dielectric-supported tubes but absent in suspended tubes. Interestingly, the suspended tubes does not show saturation due to optical phonons of the lattice of nanotube. Such a suppression in saturation is attributed to increase in current from inner-shells at higher electric-fields. Figure 6 also reveals that current density through these tubes is of the order of 10 MA/cm^2 (average current = 1 mA, average diameter = 50 nm). Copper interconnects offer current density of the order of 1 MA/cm^2 under steady state [18] and 70 MA/cm^2 [19] during ESD stress. Present work reports similar ESD current for MWCNT interconnects. This is because current through MWCNTs depends on various process parameters (diameter, number of shells, deposition technique, passivation, number of tubes etc.). Since, CNTs are resilient towards electro-migration and mean free path of scattering in CNTs is more than that in copper, improvements in the process technology can result in interconnects, which are expected to be better and robust than their copper counterparts.

From the discussion presented so far, it is clear that the surface phonon modes of the dielectric substrate plays a vital role in relieving the ESD stress by transferring the excess thermal energy from the MWCNT interconnect to the underlying dielectric substrate. However, the substrate lacks the fast-moving acoustic phonon modes, due to which thermal energy accumulates in the substrate. Therefore, for a reliable operation, MWCNT interconnects should be supported or encapsulated by a thin dielectric substrate, which can offer high thermal conductance to the heat flux from MWCNT to the global heat sink. Moreover, the choice of dielectric is also expected to affect the ESD behavior. Dielectric substrates with lower energy of surface phonons are expected to cause early saturation in current, while the substrates with relatively higher energies of surface phonon modes are expected to cause delayed saturation.

V. Conduction Through Inner Shells

Figure 7 shows ESD current conduction through inner shells of a MWCNT. Inner shells were made accessible through controlled shell-by-shell breakdown. This kind of ESD stress initiated breakdown is unique to MWCNTs and is discussed in detail in [8]. Conduction before first breakdown and second breakdown shows linear rise in current with time, while the conduction after third breakdown shows relatively less increment with time. High-bias conduction through a MWCNT takes place via tunneling across non-crossing sub-bands. Band-gap between these bands depends on diameter and is given by [15]

$$\Delta E_{NC} = 2t_0 \sin\left(\frac{\pi}{N}\right) \tag{3}$$

where, t_0 is the hopping parameter between nearest neighbor carbon atoms and N decides the diameter of the tube. Consequently, the band-gap increases with subsequent breakdowns. Although, heat propagates from hot to cold contact for every shell, the number of conduction bands smeared by

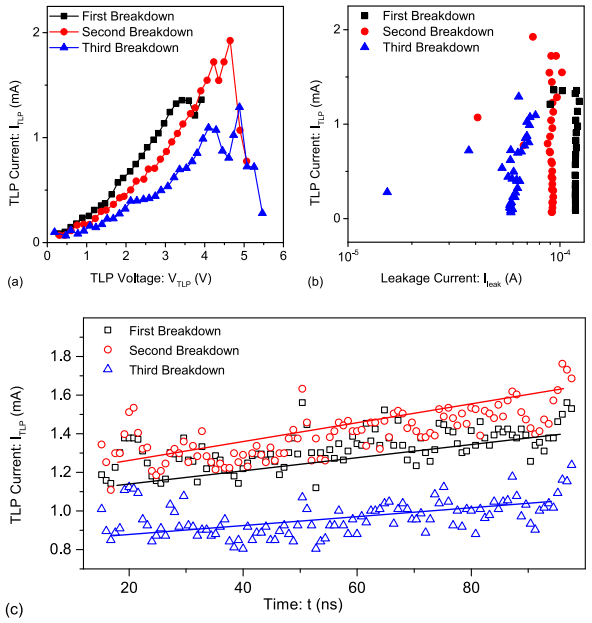

Fig. 7. (a) ESD current through inner shells; (b) fall in current through nanotubes after a particular TLP current, indicates breakdown of few outer-shells; (c) Change in ESD current with time. Note that current through outer-shells (first and second breakdown) increases with time, while current through inner shells (third breakdown) remains constant with time. Transient data is shown for TLP voltage of 4 V.

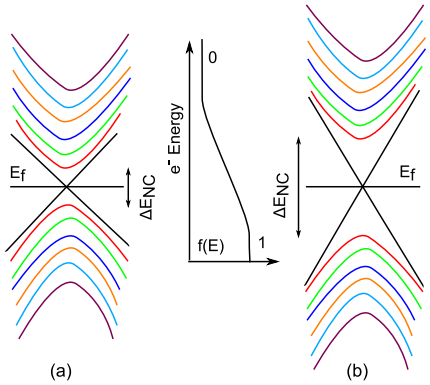

Fig. 8. Sub-bands of (a) outer and (b) inner shells of a MWCNT. Note that the number of sub-bands smeared by Fermi-Dirac distribution decreases with decrease in diameter of the shell.

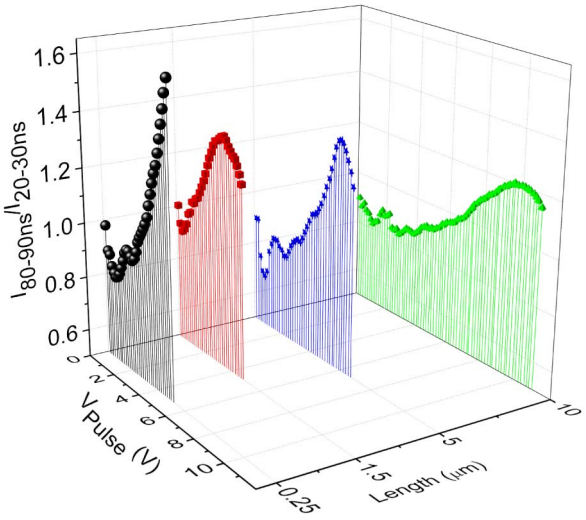

Fig. 9. Change in transient increase in ESD current with pulse voltage and length of the tube. $I_{80-90ns}$ and $I_{20-30ns}$ represents the averaging of transient current from 80 ns to 90 ns and 20 ns to 30 ns respectively.

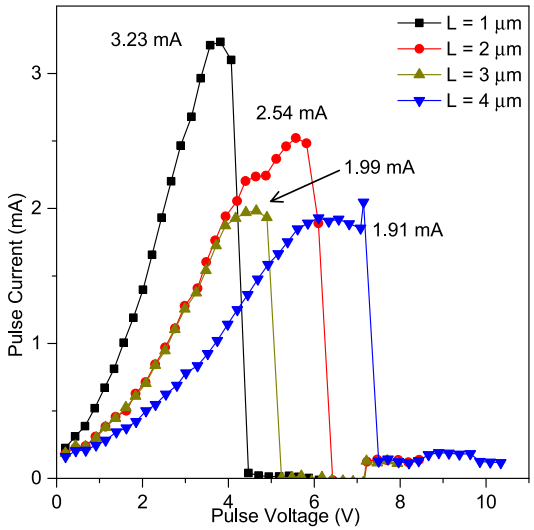

Fig. 10. Effect of length scaling on failure current and failure voltage of dielectric-supported MWCNT interconnect. Failure current decreases with length, while the failure voltage increases with the length of the interconnect.

the Fermi distribution does not increase for thinner shells (figure 8). As a result, conduction of ESD current through thick shells increases with time, but the conduction through thin shells remains relatively constant with time.

VI. Effect of Length on ESD Current

Figure 9 shows the length dependence of thermal energy assisted rise in ESD current through MWCNTs. In all the cases, after a certain threshold voltage, the current increases with time. The threshold voltage, in turn, increases with length, while the rise in current decreases with length. Overall effect is less pronounced for longer tubes. With increase in length, electrical transport through MWCNT turns from ballistic to diffusive. Less scattering in short ballistic tube paves the unimpeded rise in current with time. As a result, the upper limit of rise in current through such tubes is decided by the time taken to achieve thermal equilibrium and the sub-bands available for conduction. In diffusive tubes, scattering along the length impedes the flow of electrons and results in a reduction in transient rise in current. Consequently, the transient increase in current initially rises with voltage and then decreases after showing a peak, at which rise in current due to thermal energy gets nullified by reduction due to scattering.

Change in failure current and voltage with length of the interconnect is shown in figure 10. The failure current shows a clear reduction with increase in length of the interconnect. However, the current saturates for longer channel lengths. Failure voltage, on the other hand, increases with the length of the interconnect. The observed behavior in current can be explained by considering the rate of scattering and electric field in the MWCNT interconnect. The scattering centers

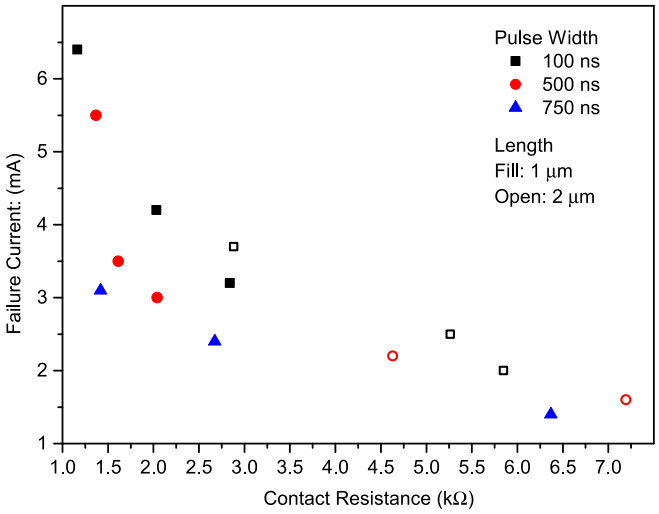

Fig. 11. Dependence of ESD current with metal-MWCNT interface resistance. The ESD current scales inversely with the contact resistance of metal-MWCNT interface. Note that the low-bias resistance, extracted after each TLP pulse, is approximated as contact resistance. This is because the individual shells provide semi-metallic path to the ESD current and most of the voltage drops across the interface.

in the MWCNT channel increases with the length, which in turn causes reduction in the current. Moreover, the reduction in electric-field increases the barrier length for Zener tunneling across non-crossing sub-bands, which also contributes to reduction in current [20]. Increase in failure voltage with length of the interconnect can be attributed to increase in thermal conductance of MWCNT-substrate interface, which increases the net heat flow to the substrate [21], which in turn delays the oxidation and eventual breakdown of the shells.

VII. ESD Current Scaling With Contact Resistance

The overall resistance of a MWCNT interconnect is composed of resistance of the channel and the resistance of the metal-MWCNT interface. The former contribution is due to the semi-metallic shells, while the latter is decided by the extent of interaction between p_z orbital of the outermost shell of MWCNT and the d orbital of metal [22]. Consequently, the overall resistance is dominated by the contact resistance of metal-MWCNT interface, and hence is expected to play a major role in deciding the ESD behavior of the interconnect. Figure 11 depicts the failure current as a function of tube resistance for two different channel lengths. As evident from the figure the failure current decreases with increase in contact resistance of the MWCNT-metal interface. This dependence can be explained by considering the change in conduction through inner shells with contact resistance of MWCNT-metal interface. With increase in the contact resistance, a substantial fraction of voltage drops across the MWCNT-metal interface and a relatively less voltage drops across the inner-shells. Moreover, the individual shells in a side-contacted MWCNT participate in conduction via inter-shell tunneling. The magnitude of inter-shell tunneling decreases with increase in inter-shell spacing [23], which in turn decreases with diameter. Consequently, there exists a non-zero inter-shell resistance [24], which increases with decrease in diameter. In presence of high contact resistance, the voltage drop across inner-shells get further suppressed due to the tunneling dependent conduction mechanism. Consequently, the electric field across outer-shells is more than the inner-shells, which in turn results in conduction of more current through outer shells than inner shells. Such a dependence on contact resistance suggests that the high-bias conduction through MWCNT with high contact resistance happen mostly through outer-shells, with the reduction in current density with decrease in diameter. A direct outcome of the contact resistance dependent conduction mechanism is the reduction in ESD reliability of MWCNT interconnects. Devices with high contact resistance force the conduction of ESD current through outer-shells only, which in turn causes increase in the population of optical phonons across the outer-shells, followed by its oxidation and early breakdown. Contrary to this, interconnects with lower contact resistance enable conduction through both inner and outer-shells, and hence relatively smaller population of optical phonons across outer-shells, which in turn delays the oxidation and breakdown of the tube. Hence, contact resistance plays a vital role in deciding not only performance of the MWCNT interconnect, but also its reliability under ESD conditions.

It is important to emphasize that fabrication of MWCNT interconnects with low contact resistance require incorporation of special contact engineering techniques in the process flow. Few of such techniques include - 1) processing end-contacted architectures [25], where the carbon atoms at the edge of the tube contacts the metal electrode 2) creating controlled defects at CNT-metal interface [22] 3) electron beam-induced deposition of graphitic carbon at CNT-metal interface [26]. Such MWCNT interconnects with low contact resistance are expected to sustain high ESD current, where the maximum value of latter is decided by contact resistance. Note that the minimum value of contact resistance of metal-CNT interface, assuming maximum interaction between p_z and d orbitals, is decided by number of conduction modes (M) available in the CNT shell contacting the reflection-less contacts [13]. Interestingly, Contact resistance of a single wall metallic CNT has a minimum value of 6.5 kΩ [26], [27]. This limitation on contact resistance is expected to put an upper limit on the magnitude of current during ESD conditions.

VIII. Wunsch-Bell Model of Failure

Thermal diffusion time for a thick MWCNT is of the order of few tens of nano seconds, which suggests that the device should attain thermal equilibrium in few nano seconds. Hence power-to-failure should not scale beyond the thermal diffusion time. Contrary to this, as shown in Fig. 12, the power to failure fits nicely to Wunsch-Bell model [28] even for the time duration much longer than thermal diffusion time. This indicates the existence of local failure sites. The entire tube, except for the local sites, could be in thermal equilibrium. The excessive heating at the local sites can result in failure or permanent damage of the tube. The carbon material fails via oxidation, which in turn follows Arrhenius model [8], [29]. According

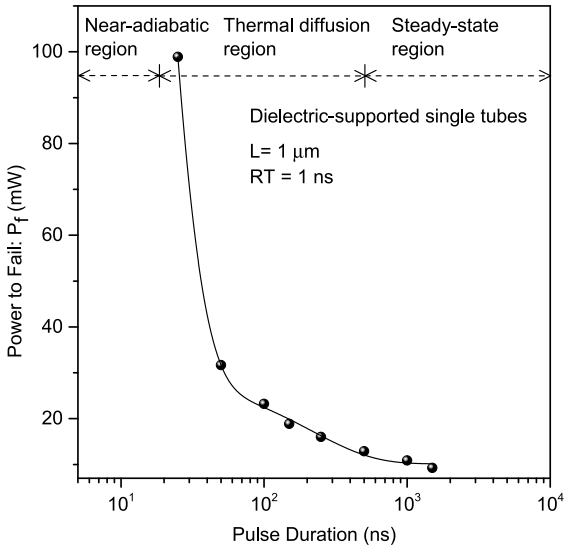

Fig. 12. Scaling of power-to-fail with pulse width. The power-to-fail depends strongly on pulse-width in thermal diffusion region, while it saturates for longer pulse-widths.

to the model, the rate of oxidation scales exponentially with temperature. Consequently, at higher local temperatures, which could be due to higher local population of optical phonons, the shells get oxidized at shorter pulse widths. Similarly, at lower local temperatures, the shells undergo slower rate of oxidation, resulting in breakdown due to longer pulses. Note that local temperature gradients or hot spots require the presence of optical phonons, which in turn requires scattering due to field induced hot carries. Consequently, as also shown by Wunsch-Bell curve in Fig. 12, there exists a minimum power-to-failure of MWCNTs.

IX. Conclusion

In summary, the coupled electro-thermal transport through MWCNT interconnects under ESD conditions was investigated by considering suspended and dielectric-supported MWCNT interconnects. Through detailed TLP analysis, ESD current through MWCNTs was traced down to sub-bands of individual shells. It was revealed that thermal energy due to high ESD stress spreads-out current to higher sub-bands and results in an increase in the device current. In dielectric-supported tubes, polar substrate takes away the thermal energy and results in relatively less ESD current, which flows only through a few lower energy sub-bands. The study shows that tubes encapsulated in thin polar materials like SiO_2 are best suited for ESD robust interconnects. The failure current was found to scale inversely with metal-MWCNT contact resistance, while the failure voltage was found to show a direct scaling with contact resistance, indicating the vital role contacts play in deciding the ESD reliability of MWCNTs.

Acknowledgment

The authors would like to thank Prof. Srinivasan Raghavan (CeNSE, IISc) and Dr. Harald Gossner (Intel) for fruitful discussions, Prof. Akshay Naik (CeNSE, IISc) and Mr. Yasasvi (CeNSE, IISc) for their support in material and device processing.

References

[1] N. Srivastava, R. V. Joshi, and K. Banerjee, "Carbon nanotube interconnects: Implications for performance, power dissipation and thermal management," in *Proc. IEEE Int. Electron Devices Meeting IEDM Tech. Dig.*, Washington, DC, USA, Dec. 2005, pp. 249–252.

[2] H. Li, W.-Y. Yin, K. Banerjee, and J.-F. Mao, "Circuit modeling and performance analysis of multi-walled carbon nanotube interconnects," *IEEE Trans. Electron Devices*, vol. 55, no. 6, pp. 1328–1337, Jun. 2008.

[3] A. A. Balandin, "Thermal properties of graphene and nanostructured carbon materials," *Nat. Mater.*, vol. 10, no. 8, pp. 569–581, Jul. 2011. [Online]. Available: http://dx.doi.org/10.1038/nmat3064

[4] B. Q. Wei, R. Vajtai, and P. M. Ajayan, "Reliability and current carrying capacity of carbon nanotubes," *Appl. Phys. Lett.*, vol. 79, no. 8, pp. 1172–1174, 2001. [Online]. Available: http://dx.doi.org/10.1063/1.1396632

[5] A. Naeemi and J. D. Meindl, "Compact physical models for multiwall carbon-nanotube interconnects," *IEEE Electron Device Lett.*, vol. 27, no. 5, pp. 338–340, May 2006.

[6] A. Nieuwoudt and Y. Massoud, "On the optimal design, performance, and reliability of future carbon nanotube-based interconnect solutions," *IEEE Trans. Electron Devices*, vol. 55, no. 8, pp. 2097–2110, Aug. 2008.

[7] G. F. Close and H.-S. P. Wong, "Fabrication and characterization of carbon nanotube interconnects," in *Proc. IEEE Int. Electron Devices Meeting*, Dec. 2007, pp. 203–206.

[8] M. Shrivastava, N. Kulshrestha, and H. Gossner, "ESD investigations of multiwalled carbon nanotubes," *IEEE Trans. Device Mater. Rel.*, vol. 14, no. 1, pp. 555–563, Mar. 2014.

[9] M. Shrivastava and H. Gossner, "ESD behavior of metallic carbon nanotubes," in *Proc. Elect. Overstress/Electrostat. Discharge Symp.*, Tucson, AZ, USA, Sep. 2014, pp. 1–6.

[10] A. Mishra and M. Shrivastava, "New insights on the ESD behavior and failure mechanism of multi wall CNTs," in *Proc. IEEE Int. Rel. Phys. Symp.*, Pasadena, CA, USA, Apr. 2016, pp. EL-8-1–EL-8-5.

[11] A. Mishra and M. Shrivastava, "Remote Joule heating assisted carrier transport in MWCNTs probed at nanosecond time scale," *Phys. Chem. Chem. Phys.*, vol. 18, no. 41, pp. 28932–28938, 2016. [Online]. Available: http://dx.doi.org/10.1039/C6CP04497B

[12] J. Moscatello *et al.*, "Surfactant-free dielectrophoretic deposition of multi-walled carbon nanotubes with tunable deposition density," *Carbon*, vol. 48, no. 12, pp. 3559–3569, 2010. [Online]. Available: http://www.sciencedirect.com/science/article/pii/S000862231000391X

[13] S. Datta, *Electronic Transport in Mesoscopic Systems* (Cambridge Studies in Semiconductor Physics). Cambridge, U.K.: Cambridge Univ. Press, 1997.

[14] S. Kaur, N. Raravikar, B. A. Helms, R. Prasher, and D. F. Ogletree, "Enhanced thermal transport at covalently functionalized carbon nanotube array interfaces," *Nat. Commun.*, vol. 5, Jan. 2014, Art. no. 3082. [Online]. Available: http://dx.doi.org/10.1038/ncomms4082

[15] M. P. Anantram, "Current-carrying capacity of carbon nanotubes," *Phys. Rev. B, Condens. Matter*, vol. 62, no. 8, pp. R4837–R4840, Aug. 2000. [Online]. Available: https://link.aps.org/doi/10.1103/PhysRevB.62.R4837

[16] K. H. Baloch, N. Voskanian, M. Bronsgeest, and J. Cumings, "Remote Joule heating by a carbon nanotube," *Nat. Nanotechnol.*, vol. 7, no. 5, pp. 316–319, 2012.

[17] S. V. Rotkin, V. Perebeinos, A. G. Petrov, and P. Avouris, "An essential mechanism of heat dissipation in carbon nanotube electronics," *Nano Lett.*, vol. 9, no. 5, pp. 1850–1855, 2009. [Online]. Available: http://dx.doi.org/10.1021/nl803835z

[18] P.-C. Wang and R. G. Filippi, "Electromigration threshold in copper interconnects," *Appl. Phys. Lett.*, vol. 78, no. 23, pp. 3598–3600, 2001. [Online]. Available: http://dx.doi.org/10.1063/1.1371251

[19] K. Banerjee, A. Amerasekera, and C. Hu, "Characterization of VLSI circuit interconnect heating and failure under ESD conditions," in *Proc. Int. Rel. Phys. Symp.*, Dallas, TX, USA, Apr. 1996, pp. 237–245.

[20] B. Bourlon *et al.*, "Geometrical dependence of high-bias current in multiwalled carbon nanotubes," *Phys. Rev. Lett.*, vol. 92, no. 2, Jan. 2004, Art. no. 026804. [Online]. Available: https://link.aps.org/doi/10.1103/PhysRevLett.92.026804

[21] E. Pop, D. A. Mann, K. E. Goodson, and H. Dai, "Electrical and thermal transport in metallic single-wall carbon nanotubes on insulating substrates," *J. Appl. Phys.*, vol. 101, no. 9, 2007, Art. no. 093710. [Online]. Available: http://dx.doi.org/10.1063/1.2717855

[22] A. Meersha *et al.*, "Record low metal—(CVD) graphene contact resistance using atomic orbital overlap engineering," in *Proc. IEEE Int. Electron Devices Meeting*, Dec. 2016, pp. 5.3.1–5.3.4.

[23] C.-H. Kiang, M. Endo, P. M. Ajayan, G. Dresselhaus, and M. S. Dresselhaus, "Size effects in carbon nanotubes," *Phys. Rev. Lett.*, vol. 81, no. 9, pp. 1869–1872, Aug. 1998. [Online]. Available: https://link.aps.org/doi/10.1103/PhysRevLett.81.1869

[24] B. Bourlon, C. Miko, L. Forró, D. C. Glattli, and A. Bachtold, "Determination of the intershell conductance in multiwalled carbon nanotubes," *Phys. Rev. Lett.*, vol. 93, no. 13, Oct. 2004, Art. no. 176806. [Online]. Available: https://link.aps.org/doi/10.1103/PhysRevLett.93.176806

[25] Y. Matsuda, W.-Q. Deng, and W. A. Goddard, "Contact resistance for 'end-contacted' metal-graphene and metal-nanotube interfaces from quantum mechanics," *J. Phys. Chem. C*, vol. 114, no. 41, pp. 17845–17850, 2010. [Online]. Available: http://dx.doi.org/10.1021/jp806437y

[26] S. Kim *et al.*, "Fabrication of an ultralow-resistance ohmic contact to MWCNT-metal interconnect using graphitic carbon by electron beam-induced deposition (EBID)," *IEEE Trans. Nanotechnol.*, vol. 11, no. 6, pp. 1223–1230, Nov. 2012.

[27] A. D. Franklin and Z. Chen, "Length scaling of carbon nanotube transistors," *Nat. Nanotechnol.*, vol. 5, no. 12, pp. 858–862, Dec. 2010. [Online]. Available: http://dx.doi.org/10.1038/nnano.2010.220

[28] S. H. Voldman, *ESD Physics and Devices*. Hoboken, NJ, USA: Wiley, 2005.

[29] P. M. Ajayan *et al.*, "Opening carbon nanotubes with oxygen and implications for filling," *Nature*, vol. 362, no. 6420, pp. 522–525, Apr. 1993. [Online]. Available: http://dx.doi.org/10.1038/362522a0

Abhishek Mishra, photograph and biography not available at the time of publication.

Mayank Shrivastava, photograph and biography not available at the time of publication.